

Peristaltic-Like Motion of the Human Fetal Right Ventricle and its Effects on Fluid Dynamics and Energy Dynamics

HADI WIPUTRA,¹ GUAT LING LIM,² KHONG CHUN CHUA,¹ R. NIVETHA,¹ SANAH MERCHANT SOOMAR,³
ARIJIT BIWAS,² CITRA NURFARAH ZAINI MATTAR,² HWA LIANG LEO,¹ and CHOON HWAI YAP ¹

¹Department of Biomedical Engineering, National University of Singapore, Singapore, Singapore; ²Department of Obstetrics and Gynecology, Yong Loo Lin School of Medicine, National University of Singapore, National University Health Systems, Singapore, Singapore; and ³Department of Paediatrics, Yong Loo Lin School of Medicine, National University of Singapore, National University Health Systems, Singapore, Singapore

(Received 17 April 2017; accepted 11 July 2017; published online 18 July 2017)

Associate Editor Dan Elson oversaw the review of this article.

Abstract—In both adult human and canine, the cardiac right ventricle (RV) is known to exhibit a peristaltic-like motion, where RV sinus (inflow region) contracts first and the infundibulum (outflow region) later, in a wave-like contraction motion. The delay in contraction between the sinus and infundibulum averaged at 15% of the cardiac cycle and was estimated to produce an intra-ventricular pressure difference of 15 mmHg. However, whether such a contractile motion occurs in human fetuses as well, its effects on hemodynamics remains unknown, and are the subject of the current study. Hemodynamic studies of fetal hearts are important as previous works showed that healthy cardiac development is sensitive to fluid mechanical forces. We performed 4D clinical ultrasound imaging on eight 20-weeks old human fetuses. In five fetal RVs, peristaltic-like contractile motion from the sinus to infundibulum (“forward peristaltic-like motion”) was observed, but in one RV, peristaltic-like motion was observed from the infundibulum to sinus (“reversed peristaltic-like motion”), and two RVs contraction delay could not be determined due to poor regression fit. Next, we performed dynamic-mesh computational fluid dynamics simulations with varying extents of peristaltic-like motions for three of the eight RVs. Results showed that the peristaltic-like motion did not affect flow patterns significantly, but had significant influence on energy dynamics: increasing extent of forward peristaltic-like motion reduced the energy required for movement of fluid out of the heart during systolic ejection, while increasing extent of reversed peristaltic-like motion increased the required energy. It is currently unclear whether the peristaltic-like motion is an adaptation to reduce physiological energy expenditure, or merely an artefact of the cardiac developmental process.

Keywords—Human fetus, Right ventricle, Peristaltic motion, Fluid mechanics, Ventricular vortex, Wall shear stress.

Address correspondence to Choon Hwai Yap, Department of Biomedical Engineering, National University of Singapore, Singapore, Singapore. Electronic mail: bieyapc@nus.edu.sg

INTRODUCTION

In both adult human and canine, it is known that right ventricle (RV) exhibits a peristaltic-like motion.^{3,13} Contractions were observed to initiate first at the RV sinus, which is near to the inflow region, and later at the infundibulum which is near the outflow tract. In between those two regions, a wave of contraction would travel from the sinus to the infundibulum in a peristaltic-like manner (Fig. 1). In the adult human, the delay in contraction between the sinus and infundibulum averaged at 15% of the cardiac cycle.³ In canine RV, the delay in contraction was estimated to produce an intraventricular pressure difference of approximately 15 mmHg between the sinus and infundibulum.¹³ However, after these initial findings, there has been little study on the topic, and the effects of the peristaltic-like motion on heart function or hemodynamics remained unknown. In fact, the existence of the peristaltic-like motion in human fetuses has yet to be confirmed.

We are particularly interested in studying the effect of this peristaltic-like motion and its influence on hemodynamics in the human fetal RV. Such mechanics studies in fetuses are important, as pointed out by evidence that suggests that the growth of prenatal heart could be affected by the fluid mechanical forces, and abnormal blood flow forces may have major contribution to development of congenital heart malformations. For example, Hove *et al.*⁵ showed that distortion of the fluid dynamics in zebra fish embryo heart by insertion of micro beads lead to malformation of the heart, Tobita *et al.*¹⁶ showed that the ligation of the left atria of chick embryos could lead to

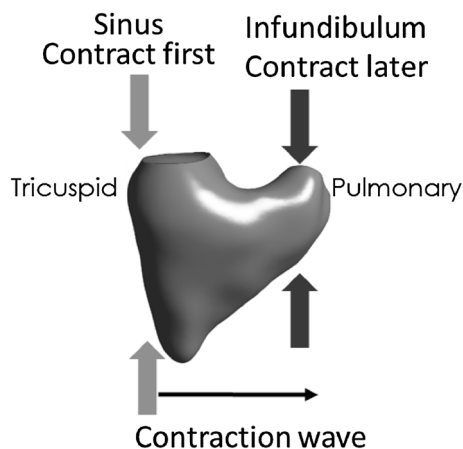


FIGURE 1. Illustration of the “forward” peristaltic-like motion, where contraction occurred first in the sinus (inlet region) and later in the infundibulum (outlet region), spreading between the two regions like a wave. A time delay in contraction between different regions can be measured.

hypoplastic left hearts, while Tworetzky *et al.*¹⁷ showed that alteration of the fluid dynamics, by dilation of the aorta, could alleviate the mal-development of hypoplastic left heart syndrome in human fetuses. Currently, however, there is insufficiency understanding of the characteristics of human fetal cardiac blood flow mechanical force environment, and their effects on fetal heart development.

In the current study, we first attempted to detect and characterize peristaltic-like motion in human fetal RV. Following which, we employed clinical ultrasound-based dynamic mesh Computational Fluid Dynamics (CFD) to assess the effect of this peristaltic-like motion on fetal RV fluid dynamics.

METHODOLOGY

The study protocol was approved by the Domain Specific Review Board of the National Health Group (Singapore) and written informed consent were obtained from all participants. Eight normal 20-weeks old fetal subjects were investigated to quantify the peristaltic-like motion, while three of the eight were used for CFD. The methods for CFD followed the procedure proposed by Wiputra *et al.*^{18,19} with modifications to incorporate the peristaltic-like motion. Detailed methodology and limitations of the technique can be found in these earlier publications.

Image Acquisition and Reconstruction

4D Ultrasound images were taken during routine checks at 20th week of gestation using Voluson 730 ultrasound machine with RAB 4-8L transducer (General Electric, Connecticut, USA). The transducer had a

frequency range of 4–8.5 MHz. Images were acquired under the 4D Spatio-Temporal Image Correlation (STIC) mode.¹²

The STIC imaging sweep occurred over 10–15 s, with image capture rate of 70–90 frames per seconds, thus giving 29–37 volumes for 1 cardiac cycle. The 4D scans were then extracted using 4DView software (General Electric, Connecticut, USA) for processing. A stack of 29 image slices perpendicular to the four chamber view were exported from the volumetric images at each time points, spaced at 0.6–0.7 mm apart. On each 2D image, the right ventricle lumen was first segmented into binary images based using the lazy snapping algorithm^{8,19} as a strategy to counter relatively high level of noise in ultrasound images. 3D reconstruction was then performed from these binary images *via* Vascular Modeling Toolkit software.¹⁵

Characterization of RV Peristaltic-Like Motion

From the 4D STIC image, 2D cine-images (image over time) of the heart at multiple regularly-spaced cross-sectional slices parallel to the apical four chamber view were extracted. Slices were labelled with increasing slice number from the RV sinus (near inlet) to the infundibulum (near outlet). We attempted to cover the entire RV, by including all slices where the lumen of the RV was visible. The cross-sectional area of the cardiac lumen over time was quantified at every cross-sectional slice.

We characterized the peristaltic-like motion by quantifying the time delay of contraction between the sinus and the infundibulum, using the workflow outlined in Fig. 2. The plot of luminal area over time for each slices was smoothed using a Fourier filter, with a cut-off frequency of the third frequency mode, resulting in a smooth graph shown in Fig. 2b. The time at which the heart achieved the maximum luminal area within a particular slice was then recorded. This time point marked the onset of contraction at that particular slice, as the area would start to decrease after reaching its maximum. Thereafter, the time point at maximum area was plotted against slice location (measured as distance from the inflow region), as shown in Fig. 2c, to investigate the trend of when different slices initiated contraction. From this figure, the delay in contraction could then be modelled *via* a linear curve-fitting. The gradient of this linearly fitted curve would signify the delay in contraction across the different slices. The total time delay between the sinus and infundibulum could also be computed by multiplying the gradient of the fitted curve with the distance between the sinus and the infundibulum.

As the measurements of the contraction delays were done with 2D planar cine-images, any translation of the

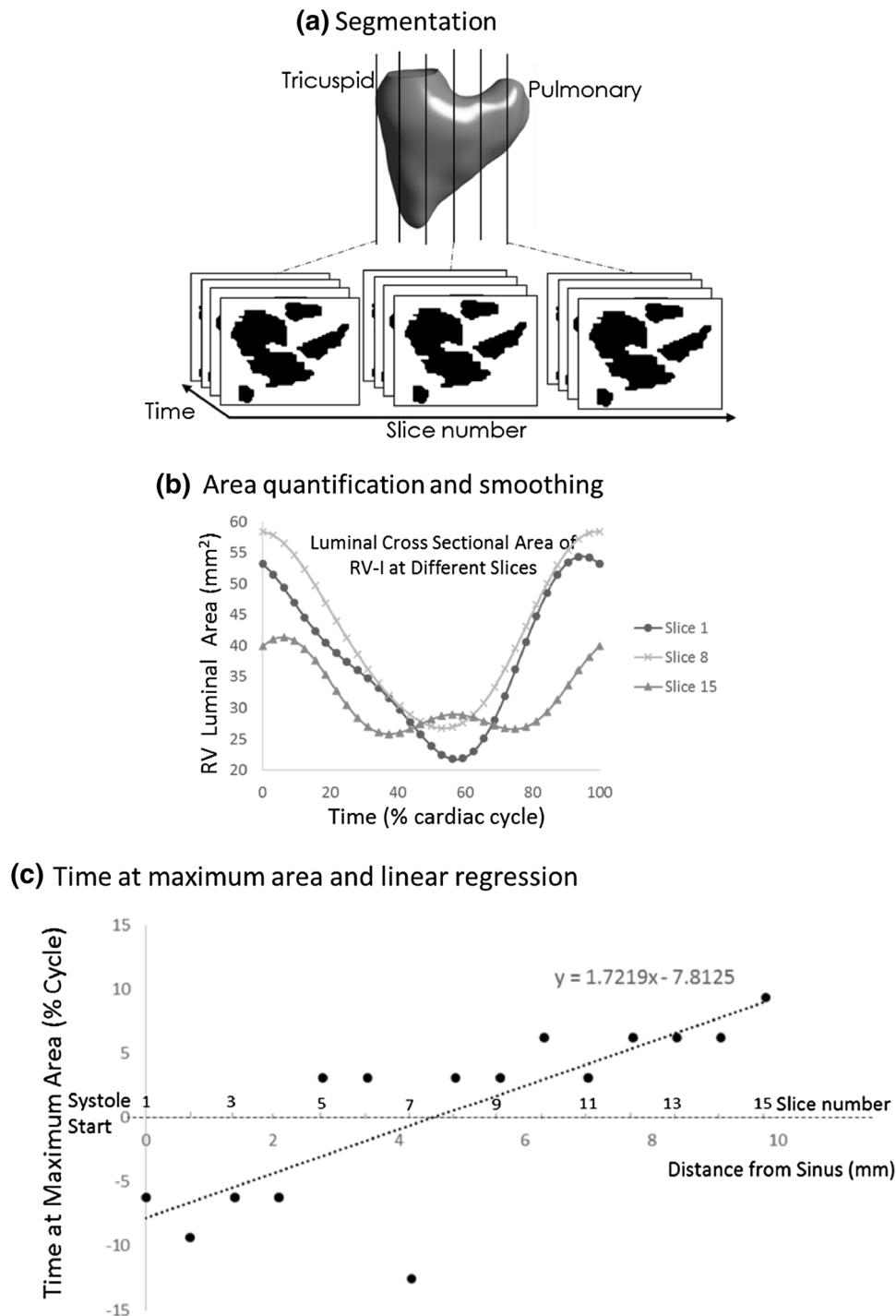


FIGURE 2. Workflow for characterization of the extent of the peristaltic-like motion, *via* quantification of the contraction delay from the RV sinus to infundibulum. (a) Segmentation of the ventricular lumen area over all time points, at multiple evenly spaced slices parallel to the four chamber view. (b) Luminal cross section area was plotted against time for each slice and smoothed *via* a Fourier filter. (c) The time at maximum area, which indicates the time of onset of contraction, was plotted against the slice number (increasing slice number were at linearly increasing distance from the RV sinus), and a linear regression line were used to model the trend.

heart in the out-of-plane direction will affect the delay values. To account for this, the out-of-plane translations were quantified, by first re-sampling the images

along the perpendicular plane, and performing cross-correlation between images from different time points. Normalised cross-correlation was computed as follows:

$$C(r, s) = \frac{1}{n} \sum_{x,y} \frac{(K(x, y) - \bar{K})(I(x + r, y + s) - \bar{I})}{\sigma_I \sigma_K}$$

where K was the kernel from the source image, chosen to be just big enough to contain the RV, I was the window of the same size on the target image, with horizontal and vertical offset of r and s pixels. σ was the standard deviation of the pixel intensity within the kernel/window, x and y were the location of the pixels, and n was the number of pixels. The (r, s) values with the highest correlation was taken to be the displacement. Maximum cumulative out-of-plane translations, however, were consistently small (<0.15 mm), and was thus neglected.

Mathematical Model of RV Wall Motion

A mathematical modelling of the RV wall motion was required to control the mesh movements in the CFD simulation of flow. The movement of the right ventricle wall was modelled by the radial displacement of each point on the surface under the spherical coordinate system, described by Eq. (1). Since the wall only moved radially, the torsion in the ventricle was not modelled, which was a limitation of the model.

$$r_{\text{model}}(\theta, \phi, t) = \alpha(\theta, \phi) * \Omega(t - \Delta t(\phi)) * u(t - \Delta t(\phi)) + r_0(\theta, \phi) \quad (1)$$

$\Omega(t)$ was the characteristic waveform that describes the radial motion, $\alpha(\theta, \phi)$ was its amplitude and $r_0(\theta, \phi)$ was the radial initial condition, obtained from the reconstructed geometry. θ and ϕ describes the azimuthal and polar angles in spherical coordinate system (depicted in Fig. 3). Differ from previous publications, Δt and u (unit step function) were added to model the contraction delay across the RV.

$\Omega(t)$ was approximated by taking the volume of the reconstructed ventricle over time to the power of 1/3, described with Fourier functions up to the eight frequency nodes. $\Omega(t)$ was then amplitude normalised, such that $\alpha(\theta, \phi)$ represented the amplitude of the radius change. The amplitude was obtained from sampling radius of RV surfaces from its centroid at the interval of 10° from 0° to 360° and 0° to 180° for θ and ϕ over time. Spherical harmonic functions were used to model $\alpha(\theta, \phi)$, in contrast with the 2D Fourier used in our previous implementation.¹⁹ This was because spherical harmonics were a better model for α at the poles of the spherical coordinates (at $\phi = 180^\circ$ and 0°) where α values must be constant across all θ values.

The peristaltic-like motion could be described as a delay in contraction at different cross-sectional slices of the heart. In Eq. (1), $\Delta t(\phi)$ was used to describe this

delay to model the peristaltic-like motion. The delay were modelled to be linear with the out-of-plane Cartesian distance from sinus slices to infundibulum slices, which could be described in spherical coordinate system as:

$$\Delta t(\phi) = \frac{D}{2} \cos(\phi) + \left| \frac{D}{2} \right| \quad (3)$$

where $\frac{D}{2}$ represented the amplitude of the contraction delay, and D was the time delay of contraction between the two ends of the RV (sinus and infundibulum), whose sign depended on the sequence of contraction (i.e. positive for sinus fist and negative for infundibulum first). Further, the unit step function (u) in Eq. (1) was added to ensure that every slice would start its motion at the correct moment within the first cardiac cycle.

For convenience, we established the naming convention for the various peristaltic-like motion cases using the contraction delay value, “ D ”. “ $D = 15\%$ ” would refer to the “forward” peristalsis case where the inlet region contracts before the outlet region by a time gap of 15% of cardiac cycle. While “ $D = -10\%$ ” would refer to the “reversed” peristalsis case where the outlet region contract earlier than the inlet region by a time gap of 10% of cardiac cycle.

To understand the effects of the peristaltic-like motion on RV flow, for one of the fetal heart dataset (RV-I), CFD was repeated for various extent of peristaltic-like motions, with the inlet-to-outlet contraction delay (D) of 15, 10, 5, 0% of cardiac cycle. The case of $D = 0\%$ of cardiac cycle referred to an absence of the peristaltic-like motion, which served as the control case. We further performed simulations on this heart with a peristaltic-like motion in the opposite direction (“the reversed peristaltic-like motion”) with inlet-to-outlet contraction delay (D) of -15 , -10 and -5% of the cardiac cycle. Two other randomly chosen fetal RVs (RV-II and RV-IV) were used to perform CFD with $D = -15$, 0 and 15% of cardiac cycle. To ensure that the comparison between different cases were conducted fairly, the stroke volumes of the different contraction delay cases were controlled to be within $\pm 1.5\%$ of the stroke volume at $D = 0\%$ case. Adjustments to the stroke volume was achieved by applying a factor to $\alpha(\theta, \phi)$. The resulting mesh motion of a case with forward peristalsis-like motion is presented as supplementary video 1.

Computational Fluid Dynamics Simulation

Dynamic mesh CFD simulations were performed with ANSYS FLUENT 16.0 (Ansys Inc., Canonsburg, PA, USA) built-in solver to solve the incompressible

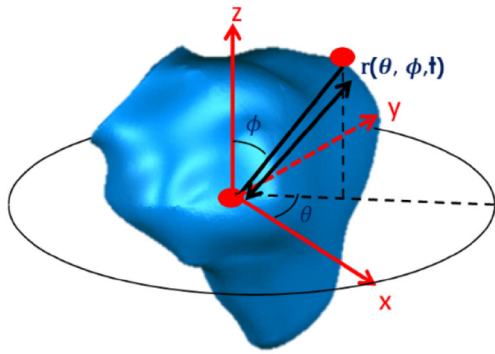


FIGURE 3. The coordinates of points on the wall of the RV were expressed in spherical coordinates.

Navier–Stokes equation, which included the continuity Eq. (4) and the momentum Eq. (5), given below:

$$\nabla \cdot \mathbf{v} = 0 \quad (4)$$

$$\rho \left(\frac{\partial \mathbf{v}}{\partial t} + \mathbf{v} \cdot \nabla \mathbf{v} \right) = -\nabla P + \nabla \cdot (\mu(\dot{\gamma}) \nabla \mathbf{v}) \quad (5)$$

where \mathbf{v} was the flow velocity, P was pressure, $\mu(\dot{\gamma})$ was non-Newtonian viscosity, as a function of shear-rate, $\dot{\gamma}$, which were described with the Carreau–Yasuda model.⁷ ρ was the fluid density. For all right ventricular models investigated, the mesh was unstructured and consisted of 1.0–1.5 million tetrahedral elements. The boundary conditions were specified as an instantaneous opening and closure of the inlets and outlets at appropriate time points, according to the timing of heart valves opening and closure. Flow into and out of the hearts during diastole and systole were brought about by the specified wall motions of the hearts. During systole, pressure at the outlet was used as the reference pressure, while during diastole, pressure at the inlet was used as the reference pressure, and pressure elsewhere in the heart were specified as differences from these reference pressures.

Simulations were run for 4 cardiac cycles to remove artefacts of the stagnant fluid initial condition and only data from the 4th cycle was presented. Each cycle was divided into 400 time steps with approximately 0.001 s per step.

Quantification of Ventricular Work Done

The systolic work done by the heart wall to induce motion in the fluid during systole (excluding work done to overcome afterload), Wd , was calculated as:

$$Wd(t) = \int_{t_0}^t \int_{CS(t)} P \cdot (\mathbf{v} \cdot \mathbf{n}) \cdot dA \cdot dt \quad (6)$$

where t_0 was the start of systole; t was the time variable, CS was the control surface, defined as the surface

enclosing the CV , i.e., RV endocardium, inlet and outlet; P was fluid pressure (expressed as pressure difference against the outlet); \mathbf{n} was the vector normal to the CS ; \mathbf{v} was the velocity vector of the CS as it moves; and A was surface area. Wd was computed as the cumulative work done by the heart that was required to bring about accelerations of fluids for ventricular ejection, and was added cumulatively from the initial value of zero at the beginning of systole.

RESULTS

Convergence Study and Comparison against Literature Value

In this study, approximately 1–1.5 million mesh elements was used. A mesh convergence study based on one heart, RV-I at $D = 0\%$, was conducted, up to a dense mesh of 3.2 million cells. Our chosen mesh density had less than 0.1% velocity error from the densest mesh. The CFD setup with 1.5 million cells was used for time-step convergence study. Our chosen time step (400 steps per cardiac cycle), was found to have ~0.11% difference from the case with smallest time steps (667 steps per cardiac cycle).

Table 1 shows the comparison of the common clinically measured parameter against the simulation result. It could be seen that generally, they are in the same order of magnitude.

Characterization of the Peristaltic-Like Motion

Careful visual inspection of the ultrasound cine-images qualitatively revealed that there were peristaltic-like motions in most hearts, where the inflow region contracted first and the outflow tract contracted later. To enable better visual inspection, the M-mode image of a line traversing the longitudinal axis of the RV at the inflow region and one at the outflow tract were reconstructed from the 4D cine-images, an example is shown in Fig. 4a. In these M-mode images, the vertical axis was distance along the line while the horizontal axis was time, and the time axis was synchronized between the two plots. It could be observed that the inflow region reached maximum size slightly earlier than the outflow tract region, demonstrating a contraction delay between the two regions (Fig. 4b). We would also like to refer to supplementary videos 2–4, which were slowed-down video of the ultrasound cine images to show the peristaltic-like motion.

Table 2 summarises the results of quantification of the peristaltic-like contraction delay for all hearts investigated. Generally, clinical fetal ultrasound images were noisy, and the R^2 values were low in some

TABLE 1. Comparison against literature values for at $D = 0\%$ for the three hearts simulated.

Cases	Stroke volume (mL)	Pulmonary Area (mm ²)	Tricuspid Area (mm ²)	Peak pulmonary velocity (m/s)	Peak E-wave velocity (m/s)	Peak A-wave velocity (m/s)
RV-I	0.44	9.6	15.7	0.422	0.215	0.375
RV-II	0.38	9.7	16.1	0.452	0.192	0.332
RV-IV	0.48	10.6	15.6	0.5512	0.279	0.3
Average	0.43 ± 0.05	9.97 ± 0.55	15.8 ± 0.3	0.476 ± 0.068	0.229 ± 0.045	0.336 ± 0.038
Literature References	0.19–0.54 9	12.5 6	19.8 1	0.46 6	0.29 ± 0.05 4	0.45 ± 0.06 4

cases. Of the eight hearts investigated, two of the hearts (RV-II and IV) were excluded from averaging due to very poor R^2 values during the curve-fitting to obtain the delay gradient, but their values were reported in Table 2 nonetheless. Of the remaining six hearts, five showed forward peristaltic-like motions, in accordance to reports in adult human and canine. Surprisingly, in one hearts (RV III), we observed reversed peristaltic-like motion. This observation was further verified with visual inspection of the cine-images (supplementary video 4), where the outlet region could be seen to contract before the inlet region. This could also be demonstrated with M-mode plots in Fig. 4c. The average forward contraction delay was found to be 12.3% of cardiac cycle, while the average reverse contraction delay was -16.6% . Combine, they gave an average delay of 7.5% cardiac cycle.

Effects of Peristaltic-Like Motion on Cardiac Fluid Dynamics

The flow structures and wall shear stress distribution were generally conserved between the different cases of peristaltic-like motion. Only minor variations were observed. Figure 5a shows the distribution of the wall shear stress and vortex structures for RV-I, under varying degrees of contraction delay ($D = -15\%$, $D = 0\%$ and $D = 15\%$). Videos of these results are also available as supplementary video 5, 7, 9 for the 3 hearts.

The Reynolds number (Re) was computed using the density, spatially-averaged maximum inflow velocity, diameter of the inlet, and viscosity. Re was found to be in the range 155–177 during peak A-wave for the three RVs. This value changed slightly across all the reverse and forward delay cases with Re of 122–131 at $D = 15\%$ and 123–143 at $D = -15\%$.

In our previous study, the dominant feature of the RV flow were the diastolic vortex rings during the E- and A-wave time points.¹⁸ These were again observed in the current study, and were common across the different D -values. Vortex rings formed at peak E and A-wave rings were observed to emanate from the tri-

cuspid inlet, and these vortex rings interacted with one another and with the RV wall. During diastole and early systole, wall shear stress elevated where the vortex structures were close to the wall, just as reported earlier.^{7,18} This was because vortices generated velocity tangential to the wall of the RV, hence generating higher shear rate at that region. During systole, in all cases, vortex structures were ejected, and high velocities at the outflow tract caused persistent high wall shear stresses there.

Minor differences in between the different peristalsis cases that were observed were as follows. During late diastole, the posterior portion of the E-wave vortex ring was less prominent in $D = 15\%$ case than in $D = 0\%$ case, which was again less prominent than in the $D = -15\%$ case. Further, at around the same time, the E-wave vortex was closer to the anterior wall and interacted more significantly with it, resulting in secondary vorticity and shear layers in that region. Due to these vortex structure differences, wall shear stress was higher in the posterior wall but lower in the superior wall directly between the RV inlet and outlet for the $D = 15\%$ case, and *vice versa* for the $D = -15\%$ case.

For more quantitative analysis, the values of the wall shear stress were averaged over the entire surface of the RV wall, and this surface-averaged wall shear stresses were plotted over time in Fig. 5b. It could be seen that compared to the non-peristalsis case, both the forward and reversed peristaltic-like motion were associated with decreases in wall shear stress values during early systole. In the forward cases, the decrease was significant, but in the reversed cases, only slight decreases were observed. During diastole, the magnitude of wall shear stresses experienced by the various peristalsis cases appeared similar, however, the non-peristalsis case experienced greater wall shear stress variability over time, while the peristaltic-like motion cases (both forward and reversed) experienced wall shear stresses versus time waveforms which were smoother.

The wall pressure distribution of the RV-I at different D -values are illustrated in Fig. 6(a). Videos of

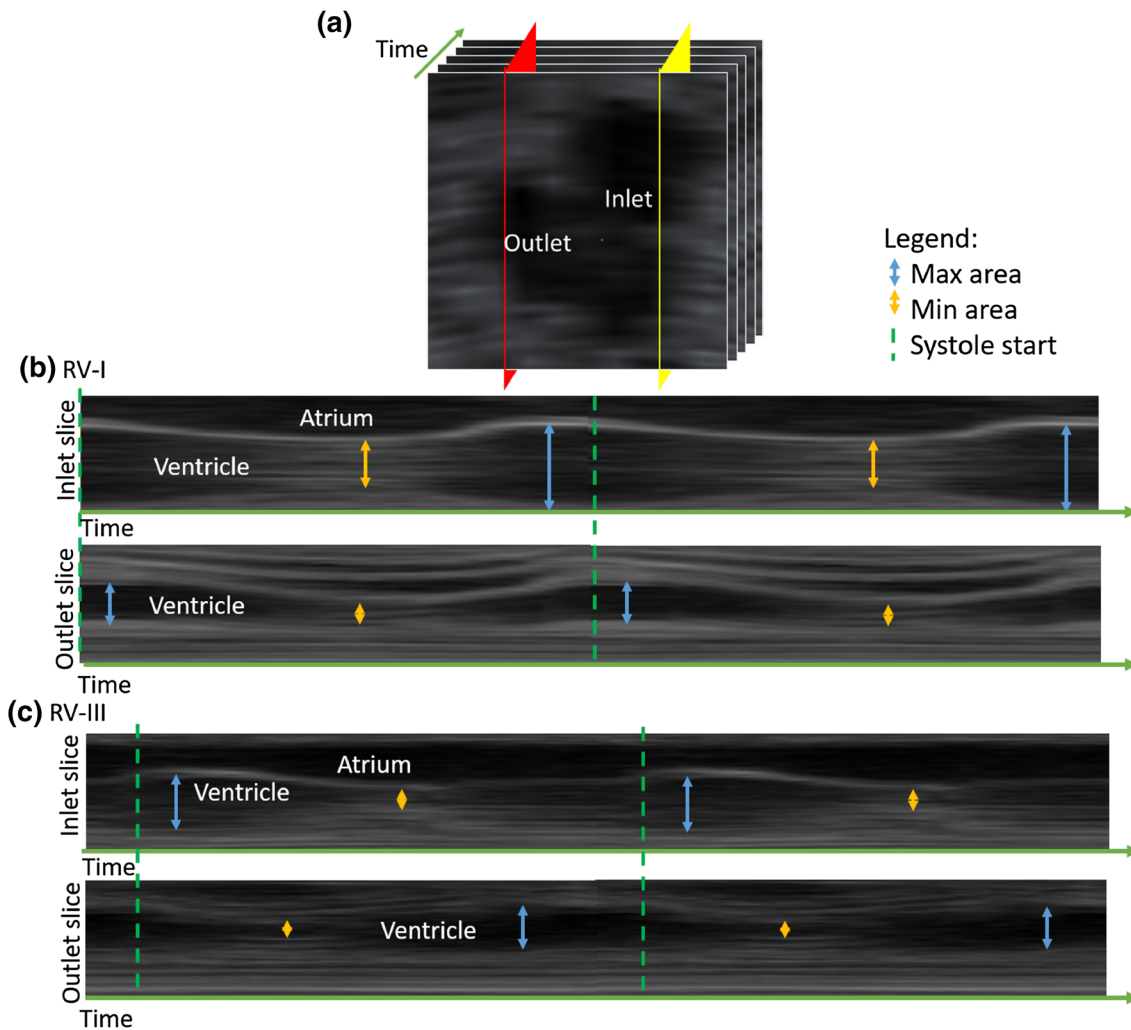


FIGURE 4. (a) Illustration of how M-mode images were extracted from the 2D cine-images for the inlet slice and outlet slice (labelled as the yellow and red plane, respectively). An M-mode image plots the pixel intensity along one line across time. (b-c) Long axis M-mode images at inlet and outlet region for (b) RV-I and (c) RV-III, plotted over 2 cycles. The green dotted lines denote the start of systole, and the blue and yellow arrow denote the approximate timing of maximum and minimum lumen size, respectively. In RV-I, the maximal area (onset of contraction) for the inlet slice occurred before the maximum area at outlet slice, however, in RV-III, the reverse was observed.

TABLE 2. Quantification of the extent of peristaltic-like motions, *via* the contraction delay (“Total delay”) between the RV inlet region and RV outlet region.

Case	Delay gradient (% cardiac cycle/mm)	Distance (mm)	Total delay (% cardiac cycle)	Total delay (ms)	R^2
RV III	-1.97	8.4	-16.5	-86.1	0.836
RV VI	0.23	9.8	2.3	9.9	0.345
RV VII	0.77	9.8	7.5	30.9	0.332
RV V	1.50	10.5	15.8	66.0	0.555
RV I	1.67	9.8	16.4	67.1	0.627
RV VIII	2.75	7.2	19.8	77.5	0.699
	Average		7.55	27.6	
	Average forward delay		12.4	50.3	
	Average reverse delay		-16.5	-86.1	
RV II**	-0.34	9.1	-3.1	-12.8	0.053
RV IV**	0.06	9.1	0.5	2.2	0.002

Positive delay values indicates contraction at the inlet region before that at the outlet region, and *vice versa* for negative delay values. The distance between the RV inlet and outlet, the delay gradient (total delay divided by Distance) and R^2 values are also shown. ** indicates cases with low R^2 values during delay gradient quantification, and were thus not included in the averaging.

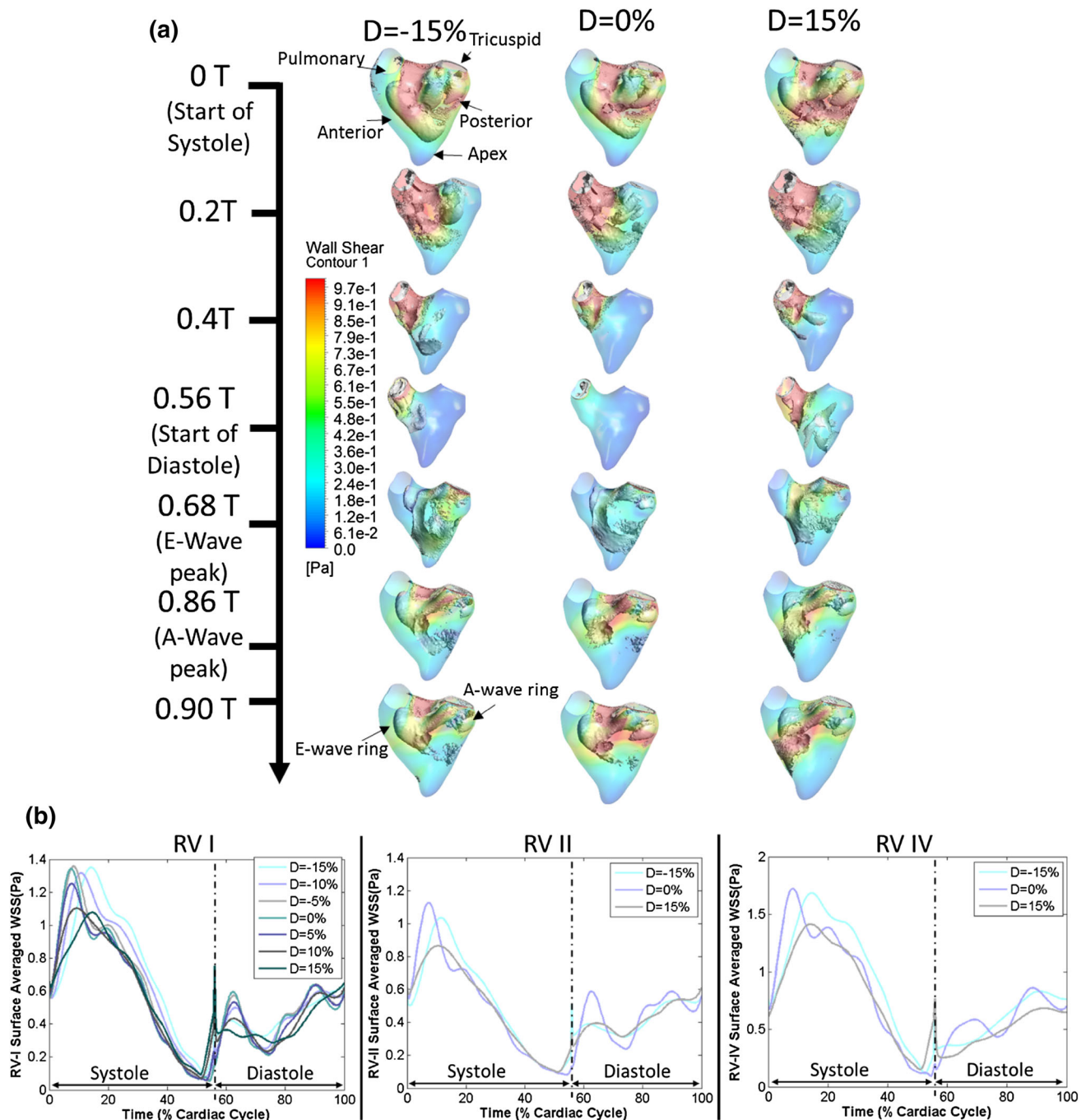


FIGURE 5. (a) Wall shear stress spatial distribution plotted concurrently with lamda 2 iso-vorticity surfaces (for vortex core visualisation), for RV-I at different extent of peristaltic-like motion (D -values), across the cardiac cycle. T refers to one period of cardiac cycle. (b) Plots of Surface averaged Wall Shear Stress of the three RVs at various contraction delay values.

these results are also available as supplementary video 6, 8, 10 for the 3 hearts. The wall pressure values were expressed as a difference with the reference values at the tricuspid inlet during diastole, and at the pulmonary outlet during systole. As such, these pressure values excluded the afterload pressure of the heart. They could be referred to as intra-ventricular pressure gradients that were responsible for the accelerations,

decelerations and movement of fluid in the heart. Generally, the pressure gradient followed the direction of acceleration and deceleration of the flow within the right ventricle, for all peristalsis cases, as was previously reported.¹⁸ For example, during systole, higher pressure manifested at the posterior wall as it was further away from the outlet and needed to accelerate fluid towards the outlet. Minor differences, however,

could be observed between the non-peristalsis case ($D = 0\%$) and the other cases, in that during the E- and A-wave deceleration phases, higher pressures inhomogeneity were experienced by the wall of the heart.

To investigate the effect of the pressure difference between the inflow and outflow region, we divided the RV into two halves along the apex, the inlet and outlet half. The difference in average pressure over the wall surface of both halves were calculated during systole. Results showed clear increased in the pressure difference with decreasing contraction delay in the forward direction (decreasing value of D), as shown in Fig. 6b. This indicated that higher pressure gradients were required to bring about systolic ejection with decreasing extent of forward peristaltic-like motions, and even higher pressure gradients were required for increasing extent of reversed peristaltic-like motions cases.

Effects of Peristaltic-Like Motion on Cardiac Energy Dynamics

Figure 7a shows the cumulative work done in different peristaltic-like motion cases to eject the same amount of blood during systole, for the 3 RVs investigated, plotted against time. From the figure, it was observed that generally, the cumulative work done decreased with increasing D . Conversely, the cumulative work done increases with increasingly negative D . This implied that forward peristaltic-like motion reduced the energy required to eject the same amount of fluid out of the RV, while reversed peristaltic-like motion increased the energy required to do so. A minor deviation was the case of RV-II, where the work done for fluid ejection in the case of $D = -15\%$ was only marginally higher than (less than 1%) case of $D = 0\%$. Averaged across the three RVs, the work done at $D = 15\%$ was 16.1% lower than $D = 0\%$, while the work done at $D = -15\%$ was 9.1% higher than $D = 0\%$ case. The systolic work done calculation results of all peristalsis cases were plotted in Fig. 7b. The results clearly reinforced the notion that forward peristalsis reduced work done required for systolic ejection while reverse peristalsis cases increased it, in a manner that depended on the extent of the peristaltic-like motion.

It is noteworthy that across all the various contraction delay settings tested, the volumetric kinetic energy remains relatively unaffected, with the different cases having kinetic energy versus time plots with similar shapes and similar peak kinetic energy values. As the majority of the flow dynamics was dominated by the vortices, this observation corroborated with the observation that only minor changes in vortex dynamics were observed between the different peristalsis cases.

DISCUSSION

In this study, we confirmed the presence of a peristaltic-like motion in the fetal right ventricle, and found that while this motion caused only minor changes in flow dynamics (flow patterns, vortex dynamics and wall shear stresses), there were significant changes to the energy dynamics of systolic ejection.

We first highlight that the term “peristaltic-like motion” is not synonymous with peristaltic motion. The heart lumen does not complete collapse during its contraction, and it thus clearly does not undergo peristalsis. This term is used merely because it is a convenient way of describing the wave-like motion, which is also easy to understand.

The observed changes to flow dynamics between cases with and without the peristaltic-like motion were caused by the changes to wall motions. In the case with no peristaltic-like motion, all of the RV wall moved in and out in unison, causing fluid everywhere in the ventricle to move away from the inlet or towards the outlet in a coordinated fashion. However, in the cases with peristaltic-like motions, the wall motion at different locations of the heart were offset in time. Consequently, fluid moved from one part of the heart to another (from the contracting region into the region with delayed contraction), and ejection or inflow occurred in a somewhat segmented fashion. This would obviously cause changes to the vortex structures and wall shear stress spatial patterns, but changes were observed to be minor.

The difference between coordinate and segmented fluid motion could explain the observed higher systolic wall shear stresses in the non-peristalsis case (Fig. 5). The coordinated movement of fluid towards the outflow tract brought about a “rush-hour congestion”, causing greater fluid velocity within a shorter duration, and thus greater interaction of fluid with the walls and higher wall shear stresses. On the other hand, the segmented fluid motion had the effect of spreading out the occurrences of high velocities and fluid-wall interaction over time, thus reducing wall shear stresses, and causing a smoothing effect on wall shear stress over time waveform, could also be observed in plots in Fig. 5b (especially during mid- to late diastole).

Comparing the forward versus reversed peristaltic-like motion cases, in the positive D -valued cases, the outlet region contracted later than the inlet region, but this was reversed for the negative cases. Consequently, the reversed cases had outflow tracts with smaller cross-sectional areas at the time when peak systolic flow manifested. This resulted in higher systolic wall shear stresses in the reversed cases than forward cases.

The coordinated versus segmented manner of fluid motion within the RV could also explain the wall

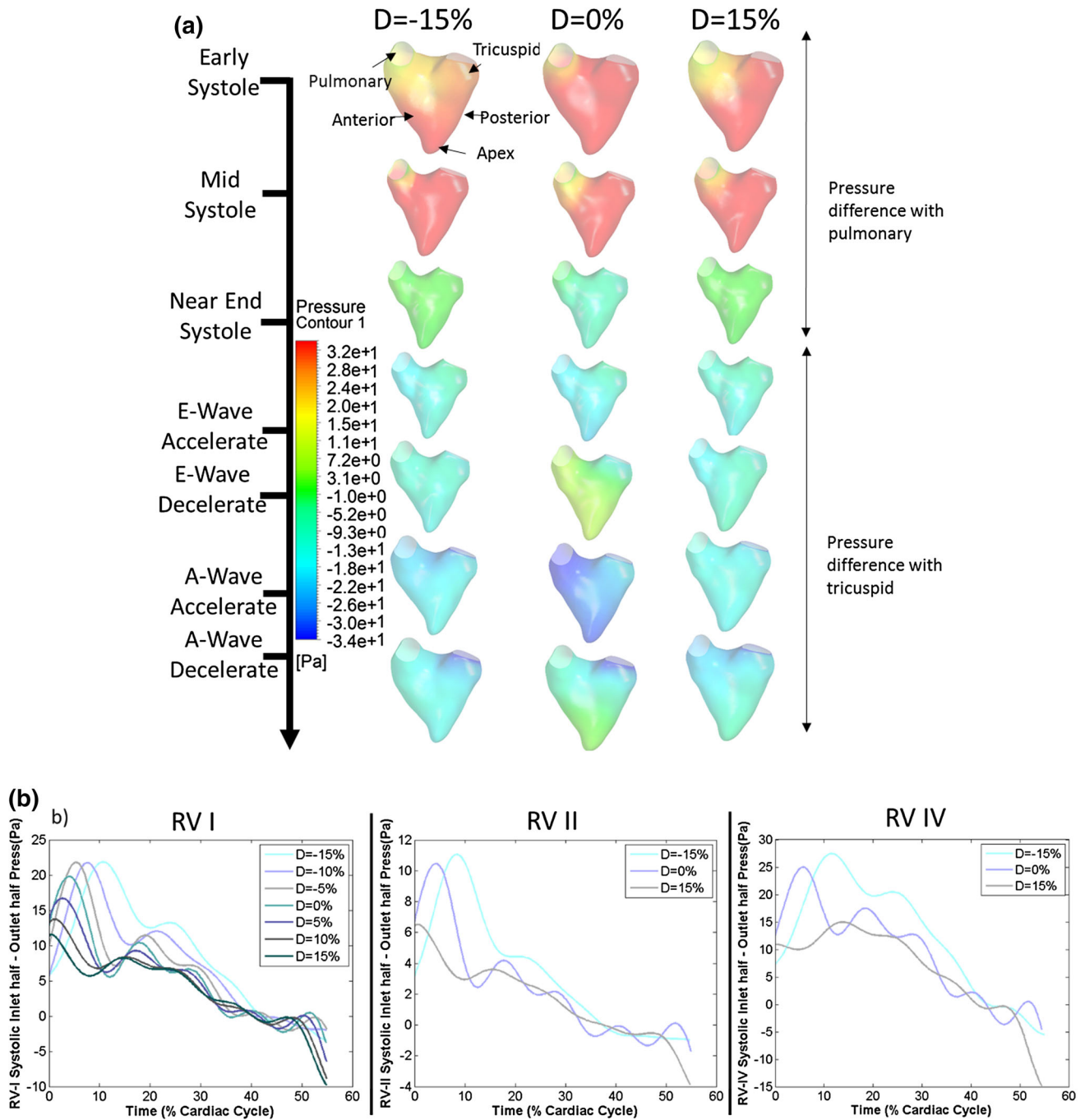


FIGURE 6. (a) Wall pressure distribution across the cardiac cycle for the simulated RV-I at $D = 15\%$, $D = 0\%$ and $D = -15\%$. (b) Plots of systolic surface-averaged pressure gradient (Inlet half minus outlet half) for different D values for RV I, II and IV.

pressure results, shown in Fig. 6a. At certain time points, the non-peristalsis case showed greater spatial inhomogeneity of wall pressures, for example, during the deceleration phases of the E- and A-wave. Further, pressure gradient versus time plots in Fig. 6b also demonstrated greater variability over time for the non-peristalsis cases, compared to both forward and reversed peristalsis cases. The segmented manner of fluid

motion had the effect of spreading out pressure gradients over time, resulting in reduced spatial inhomogeneity at any one time point, and resulting in smoothing pressure over time plots. The role of the peristaltic-like RV motion in manipulating pressure was previously proposed by Amour *et al.*² Armour *et al.* however, had a different way of explaining it, describing the outlet portion of the RV as a pressure

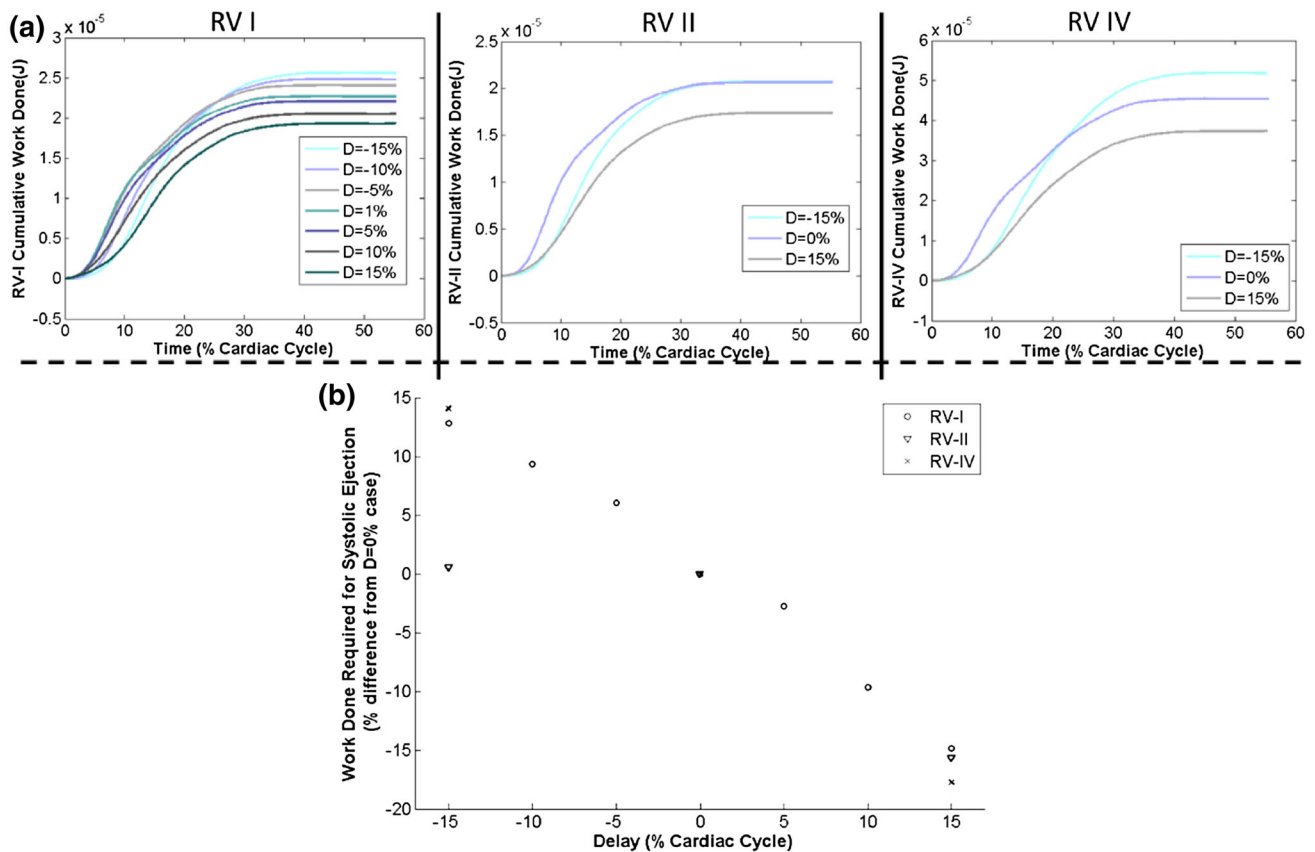


FIGURE 7. (a) Cumulative Work done over systole, (b) Percent changes in the systolic work done at different D -values for all the three RVs investigated.

regulator, which modulated the pressure gradient between the sinus and the pulmonary outflow generated by sinus contractions.

Our simulation results also showed that forward peristaltic-like motion cases required less energy to move fluid out of the heart during systolic ejection, compared to reversed peristaltic-like motion cases. The energy savings could be substantial: the $D = 15\%$ forward peristaltic-like motion case reduced energy required for ejecting fluid by 16%, while the $D = -15\%$ reversed peristaltic-like motion case increased energy required by up to 9%. The forward case thus enjoyed a 25% reduced viscous energy losses during ejection.

The mechanism by which energy loss was reduced can be understood by the notion that the forward peristaltic-like motion was equivalent to a peristaltic effort to channel flow towards the outlet during systole, while the reversed peristaltic-like motion was equivalent to one that channelled flow towards the inlet. The latter would obviously be less fruitful, since systole involved ejection, not inflow. Another way to understand this was to consider the cross-sectional sizes of the various parts of the RV. Since the reversed

motion constricted the outlet region first, ejection flow would have to go through narrower outlet channels to exit the heart, resulting in more frictional viscous energy losses. Conversely, the forward motion constricted the outlet region last, enabling ejecting flow to pass through wider outlet channels, resulting in reduced energy losses. A simple analogy could be that of squeezing the toothpaste tube. One would find it easier to get all the toothpaste out of the tube if one were to squeeze the far end first, rather than to start squeezing at the region near to the tube outlet.

Further, the wall shear stresses and pressure gradient results corroborated with the energy loss results, and could explain the mechanism causing the difference in energy dynamics. Since the forward motion cases had lower systolic wall shear stresses than reversed motion cases (Fig. 5), less frictional viscous energy losses occurred at the walls, thus reducing energy requirements for ejection. Also, since higher pressure gradients (Fig. 6) were required by the reversed motion cases for ejecting the same amount of fluid than the non-peristalsis case, which in turns required more pressure than the forward motion cases, it followed that the energy losses were higher in the

reversed cases, followed by the non-peristalsis case, followed by the forward cases.

In RV-II, however, an anomaly was observed. The cumulative systolic work done by $D = -15\%$ case was only marginally higher than $D = 0\%$. In all other hearts used for CFD, the increase was significantly higher. This was most likely caused by geometric differences: RV-II had a larger infundibulum than the other two hearts. With a larger infundibulum, early contraction of the outflow tract during systole (in the reverse peristaltic-like motion case) would not lead to significantly more energy losses and thus work done for ejection.

Our study filled in the gap in the literature on the existence of the peristaltic-like motion of the RV in fetuses. Since the peristaltic-like motion is now reported for both fetuses and adults, we can establish that they are features established by cardiac development. It has been suggested that the motion's existence may be an artefact of the developmental stages of the heart when it was a tube,^{1,3} where the entire heart, including the RV, was linear, and relied on peristalsis for fluid pumping.¹⁰ Further, we noted that the inlet portion (sinus) and the outflow tract (infundibulum) developed separately. The infundibulum developed earlier, at 20 days post fertilisation, while the sinus developed a few days later from the proximal bulbus cordis.¹¹ This could have caused differential timing of contraction of different regions of the RV.

More directly, the mechanism responsible for the presentation of the peristaltic-like motion was most likely the RV's conduction system architecture, as this directly controlled the timing of contraction of different parts of the RV myocardium. The architecture could feature shorter neural paths to the sinus region or to the infundibulum region to lead to the differential contraction timing. An earlier study demonstrate that electrical mapping of the adult human RV showed a slight delay in the activation of the muscles near the right ventricle outflow tract,¹⁴ providing evidence of this mechanism. Further, it is likely that the conduction system architecture of the 20 weeks old fetal RV might be preserved into adulthood, and that the same peristaltic-like motion found in the fetal heart would persist into adulthood, but this might be difficult to confirm.

Our finding that the forward peristaltic-like motion could reduce energy expenditure associated with fluid ejection naturally posed the hypothesis that this feature could be an adaptation of the heart to save energy and gain survival advantages. However, the existence of reversed peristaltic-like motion cases in our cohort of 8 fetal hearts posed a serious challenge to this hypothesis. This was especially so when all our fetal subjects were healthy. To the best of our knowledge, reverse peristaltic-like motion of the RV has never been

reported. In the study on canine hearts, one of the six canine hearts studied did not have an early systolic expansion of the outflow tract,¹³ and could be a reversed peristaltic-like motion case, but the authors made no mention of such a motion.

One possible way to analyse the delay values of the 6 hearts in Table 2 was to investigate the statistical distribution of the delay gradient values. *Via* the Anderson–Darling test, we determined that there was not sufficient evidence to reject the hypothesis that the data followed a normal distribution, at 0.05 significance level. Under this line of thought, the reversed peristaltic-like motion was not an anomaly but merely a statistical variation, with unknown but potentially interesting physiological origins. The opposing view is that the reversal of the peristaltic-like motion is a major change, and it would not be appropriate to analyse it purely based on statistics.

LIMITATION

We acknowledge the following limitations in this study. We used a simplified linear model for the contraction delay distribution along a single direction. In actuality, the delay distribution could be 3D and non-linear, and might not be one-directional. However, we observed that the peristaltic-like motion was most significant and easily observable in the direction between the sinus and infundibulum, and this was also reported for adults in previous studies.^{3,13} The study also had limitations in its CFD implementations, which were detailed in our previous publications.^{18,19}

CONCLUSION

We report evidence of peristaltic-like motion in fetal cardiac right ventricles. In the majority of cases, the peristaltic-like motion was in the “forward” direction, from the inlet region to the outlet region. Our study also indicated that forward peristaltic-like motion reduced energy loss of ejection flow, and reduced the required work done for systolic ejection, in a linear dependency with the extent of the peristaltic-like motion. In the same way, reversed peristaltic-like motion increased energy loss and required work done for systolic ejection with the same dependency on the extent of the motion.

ELECTRONIC SUPPLEMENTARY MATERIAL

The online version of this article (doi: [10.1007/s10439-017-1886-5](https://doi.org/10.1007/s10439-017-1886-5)) contains supplementary material, which is available to authorized users.

ACKNOWLEDGEMENTS

The authors thank the National University of Singapore Young Investigator Award, grant entitled “Fluid Mechanics and Mechanobiology of Congenital Cardiac Outflow Tract Malformations” (PI: Yap) for funding, and the National University of Singapore Graduate School of Integrated Sciences and Engineering Scholarship for funding support for the lead author, Hadi Wiputra.

REFERENCES

- ¹Allan, L., S. K. Chita, W. Al-Ghazali, D. Crawford, and M. Tynan. Doppler echocardiographic evaluation of the normal human fetal heart. *Br. Heart J.* 57:528–533, 1987.
- ²Armour, J., J. Pace, and W. Randall. Interrelationship of architecture and function of the right ventricle. *Am. J. Physiol.-Leg. Content* 218:174–179, 2016.
- ³Geva, T., A. J. Powell, E. C. Crawford, T. Chung, and S. D. Colan. Evaluation of regional differences in right ventricular systolic function by acoustic quantification echocardiography and cine magnetic resonance imaging. *Circulation* 98:339–345, 1998.
- ⁴Harada, K., M. J. Rice, T. Shiota, M. Ishii, R. W. McDonald, M. D. Reller, and D. J. Sahn. Gestational age- and growth-related alterations in fetal right and left ventricular diastolic filling patterns. *Am. J. Cardiol.* 79:173–177, 1997.
- ⁵Hove, J. R., R. W. Koster, A. S. Forouhar, G. Acevedo-Bolton, S. E. Fraser, and M. Gharib. Intracardiac fluid forces are an essential epigenetic factor for embryonic cardiogenesis. *Nature* 421:172–177, 2003.
- ⁶Kenny, J. F., T. Plappert, P. Doubilet, D. H. Saltzman, M. Cartier, L. Zollars, G. Leatherman, and M. S. J. Sutton. Changes in intracardiac blood flow velocities and right and left ventricular stroke volumes with gestational age in the normal human fetus: a prospective Doppler echocardiographic study. *Circulation* 74:1208–1216, 1986.
- ⁷Lai, C. Q., G. L. Lim, M. Jamil, C. N. Z. Mattar, A. Biswas, and C. H. Yap. Fluid mechanics of blood flow in human fetal left ventricles based on patient-specific 4D ultrasound scans. *Biomech. Modeling Mechanobiol.* 15:1159–1172, 2016.
- ⁸Li, Y., J. Sun, C. K. Tang, and I. Y. Shum. Lazy snapping. *Acm Trans. Graph.* 23:303–308, 2004.
- ⁹Molina, F., C. Faro, A. Sotiriadis, T. Dagklis, and K. Nicolaidis. Heart stroke volume and cardiac output by four-dimensional ultrasound in normal fetuses. *Ultrasound Obstet. Gynecol.* 32:181–187, 2008.
- ¹⁰Moorman, A. F., F. De Jong, M. M. Denyn, and W. H. Lamers. Development of the cardiac conduction system. *Circu. Res.* 82:629–644, 1998.
- ¹¹Moss, A. J., and F. H. Adams. Heart Disease in Infants, Children, and Adolescents. Baltimore: Williams & Wilkins Company, 1968.
- ¹²Paladini, D., M. Vassallo, G. Sglavo, C. Lapadula, and P. Martinelli. The role of spatio-temporal image correlation (STIC) with tomographic ultrasound imaging (TUI) in the sequential analysis of fetal congenital heart disease. *Ultrasound Obstet. Gynecol.* 27:555–561, 2006.
- ¹³Raines, R., M. LeWinter, and J. Covell. Regional shortening patterns in canine right ventricle. *Am. J. Physiol.-Leg. Content* 231:1395–1400, 1976.
- ¹⁴Ramanathan, C., P. Jia, R. Ghanem, K. Ryu, and Y. Rudy. Activation and repolarization of the normal human heart under complete physiological conditions. *Proc. Natl. Acad. Sci.* 103:6309–6314, 2006.
- ¹⁵Steinman D. and L. Antiga. VMTK-Vascular Modeling Toolkit. Webpage, 2008.
- ¹⁶Tobita, K., and B. B. Keller. Right and left ventricular wall deformation patterns in normal and left heart hypoplasia chick embryos. *Am. J. Physiol. Heart Circ. Physiol.* 279:H959–H969, 2000.
- ¹⁷Tworetzky, W., L. Wilkins-Haug, R. W. Jennings, M. E. van der Velde, A. C. Marshall, G. R. Marx, S. D. Colan, C. B. Benson, J. E. Lock, and S. B. Perry. Balloon dilation of severe aortic stenosis in the fetus potential for prevention of hypoplastic left heart syndrome: candidate selection, technique, and results of successful intervention. *Circulation* 110:2125–2131, 2004.
- ¹⁸Wiputra, H., C. Q. Lai, G. L. Lim, J. J. W. Heng, L. Guo, S. M. Soomar, H. L. Leo, A. Biwas, C. N. Z. Mattar, and C. H. Yap. Fluid mechanics of human fetal right ventricles from image-based computational fluid dynamics using 4D clinical ultrasound scans. *Am. J. Physiol.-Heart Circ. Physiol.* 311:H1498–H1508, 2016.
- ¹⁹Wiputra, H., G. L. Lim, D. A. K. Chia, C. N. Z. Mattar, A. Biswas, and C. H. Yap. Methods for fluid dynamics simulations of human fetal cardiac chambers based on patient-specific 4D ultrasound scans. *J. Biomech. Sci. Eng.* 11:15, 2016.